Field testing on foundation damping for offshore wind turbines supported by large diameter monopiles

Y. Zhang
Southeast University, Nanjing, China, youhuzhang@seu.edu.cn

P. Guo, G. Tian, Y. Huang
Southeast University, Nanjing, China, guopeng1126@seu.edu.cn, tiangp@seu.edu.cn, yinghuang@seu.edu.cn

T. Qi, W. Ji, R. Li, R. Yan
Goldwind Sci & Tech Co., Ltd., Beijing, China, qitao33085@goldwind.com, jiweidong@goldwind.com, lirongfu@goldwind.com, yanruiyang@goldwind.com

E. Anderson, P. Sparrevik, A. Page
Norwegian Geotechnical Institute, Oslo, Norway, emily.anderson@ngi.no, per.sparrevik@ngi.no, ana.page@ngi.no

ABSTRACT: Foundation damping holds considerable potential for the design optimisation of monopile-supported offshore wind turbine structures. In recent years, various models have been developed to quantify foundation damping, and its influence on system dynamics has been investigated using integrated time-domain analyses. However, physical model testing and experimental validation of such models remain scarce. To address this gap, a series of field-based, medium-scale physical model tests were conducted at a homogeneous marine clay site near the coast. The monopile foundation, tower structure and wind turbine system were scaled following a geometric scaling ratio of 1:10. The testing programme comprised monotonic loading tests, free-vibration tests and frequency sweep tests conducted under different load amplitudes. This paper presents representative experimental results together with preliminary interpretation.

1 INTRODUCTION

Monopiles remain the dominant foundation solution for offshore wind turbines, accounting for approximately 67% of the global installed capacity for projects in operation by the end of 2024 and about 62% of those currently under construction (GWEC, 2025). However, the expansion of offshore wind developments into deeper waters and the deployment of larger turbines have imposed increasingly more stringent demands on foundation stiffness and bearing capacity, resulting in substantial increases in monopile diameter and embedment length and associated challenges for fabrication and installation. In response, considerable efforts have focused on improving the modelling of soil–pile interaction stiffness and capacity (e.g., Suryasentana and Lehane, 2016; Zhang and Andersen, 2017, 2019; Burd et al., 2020a, 2020b; Byrne et al., 2020; Fu et al., 2020; Lai et al., 2020), enabling more optimised monopile and tower designs and extending their applicability to a wider range of water depths and ground conditions. In contrast, foundation damping, although potentially important for the dynamic response of offshore wind turbine structures (OWTs), is not explicitly accounted for in current engineering design practice.

In recent years, various models have been developed to calculate foundation damping (e.g., Page, et al., 2019, Zhang et al., 2021, Barzan and Igoe, 2024, Shirzoi et al., 2024, Guo et al., 2025) and its impact on system dynamics have been investigated by integrated time domain analyses (Fontana et al., 2015, Page et al., 2019, Rezaei et al., 2018, and Linde and Saeland, 2022, Carswell et al., 2015, 2022, Guo et al., 2024a, 2024b, 2024c). The aforementioned studies are mostly based on numerical modelling. Physical model testing and validation of such models remain scarce (Jindal et al., 2024a, 2024b).

Over the last few years, the authors have conducted systematic investigations into foundation damping and its load-reduction effects, and have proposed an innovative approach to directly obtain foundation damping at the *p–y* spring level by mapping damping ratios from the soil element level. Furthermore, integrated aero-servo-hydro-elastic analyses performed using Bladed and OpenFAST have demonstrated that foundation damping holds considerable potential for design optimisation of monopile-supported offshore wind turbines (Zhang et al., 2021, 2023, Guo et al., 2024a, 2024b, 2024c, 2025a, 2025b, Ji et al., 2025, Page, et al., 2019). To bridge the gap between theoretical developments and practical application, a series of field tests were conducted to validate the theoretical models.

This paper presents representative results from the field tests together with preliminary interpretations. The focus is on reporting the test data, while their back-analysis and comparison with theoretical models will be addressed in future publications. The test results demonstrate that the testing programme was successfully completed, yielding high-quality data that provide a solid basis for further interpretation and validation of the previously developed methods.

2 SPECIFICATION OF THE TEST PROGRAMME

2.1 Test site

The field tests were conducted on Lingkun Island, Wenzhou, Zhejiang Province, China, approximately 1 km inland from the coastline. Groundwater table was encountered at a depth of about 0.5 m below the ground level. Table 1 presents physical properties measured on selected soil samples.

Table 1. Selected physical properties of the soil samples.

No.	Depth (m)	Water content (%)	Unit weight (kN/m^3)	Plasticity index (%)	Clay particles (%)
1	2~2.5	39.5	18.0	21.4	27.0
2	3~3.5	44.7	17.4	20.0	28.0
3	3.5~4	36.6	18.3	19.6	16.5
4	4~4.5	40.8	17.8	17.8	21.8
5	5.5~6	49.1	17.0	20.9	20.8
6	6~6.5	46.2	17.3	25.4	30.4
7	15.5~16	55.8	16.5	25.8	27.0

The site was investigated using cone penetration tests with pore pressure measurements (CPTU) and borehole drilling, complemented by a systematic programme of laboratory soil element testing. The site investigation reveals highly consistent soil conditions across the testing site. Up to to 30 m below the ground surface, the site mainly consists of medium plasticity, lightly over-consolidated silty clay. Figure 1 presents the intepreted undrained shear strength (s_u) and over-consolidation ratio (*OCR*) profiles based on CPTU results and laboratory testsing, with OCR interpreted using k = 0.3. Between 6-14 m, spiky CPTU responses are noted which is due to presence of very thin (typically 2-5 mm in thickness) silty sand seams embeded in the clay matrix.

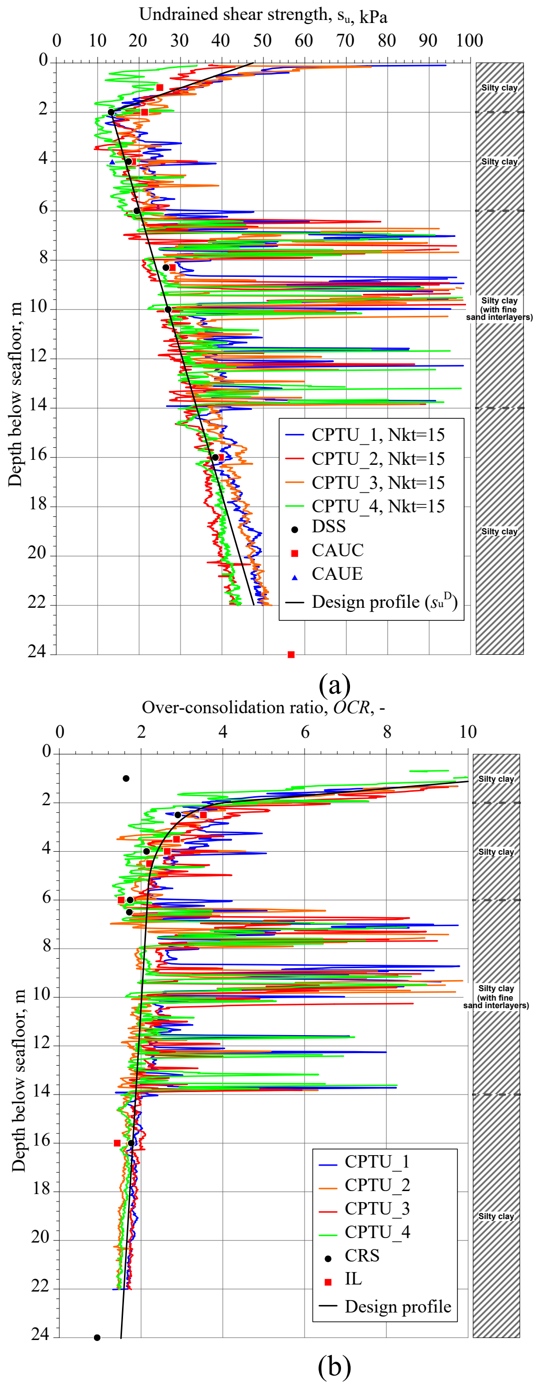

Figure 1. (a) undrained shear strength s_u (b) overconsolidation ratio. CAUC: consolidated undrained triaxial compression test; CAUE: consolidated undrained triaxial extension test; DSS, direct simple shear test; CRS: constant rate of strain oedometer test; IL: Incremental loading oedometer test.

2.2 Test set-up

Figure 2 illustrates the layout of the test site. One reaction pile was installed, together with four surrounding testing piles in a circular arc configuration. After testing of the first four piles (Piles A-D), the reaction pile was relocated for testing of Pile E and Pile F. The centre-to-centre spacing between the reaction pile and each of the testing piles was kept at 8 m. The diameter (D) of the reaction pile and testing pile is 2.5 and 1.0 m, respectively. The reaction pile has a total length of 15m, while five of the testing piles have a length of 9 m and one remaining testing pile has a length of 13 m. The tower has an outer diameter of 0.7 m and a total length of 12 m. The lumped mass is a solid cylindrical block with a height of 255 mm and a weight of 800 kg. The dimensions and mass properties of the tower and the lumped mass were based on a prototype 12 MW wind turbine and scaled according to a geometric scale factor of 1:10.

For the reaction pile, a YZ-280L vibratory hammer was used to install the pile to the target embedment depth of 12 m. For the testing piles, a YZ-90D vibratory hammer was first employed to install the piles to a depth of 3 m to ensure stability. The piles were then driven to a target depth of 7 m (for 9 m long piles) and 11 m (for 13 m long piles). Following installation, the test piles were left undisturbed for at least one month to allow for recovery of the soil-pile interface. It should be noted that, prior to testing, a 1 m deep excavation was carried out around the testing piles to eliminate the influence of the surface crust. The effective embedment (L) to diameter (D) ratio is thus 6 and 10 for the short and long testing piles, respectively.

Figure 2. Layout of the test site, test piles and reaction pile

The field testing programme comprised three main categories of tests: (i) loading tests without the superstructure, including monotonic and cyclic loading tests; (ii) free-vibration tests with the superstructure; and (iii) forced excitation tests with the superstructure, as illustrated in Figure 3. The testing system consisted of a reaction pile, a testing pile, an servo actuator, a tower, a lumped mass repreenting the wind turbine, a control system, a data acquisition system, and a monitoring system. Details of the system configuration are shown in Figure 3.

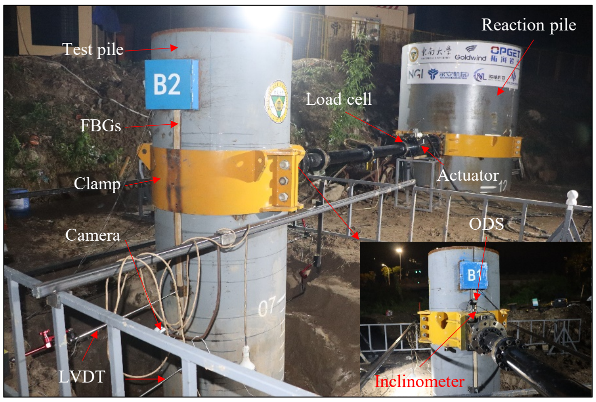

(a) Loading tests without superstructure

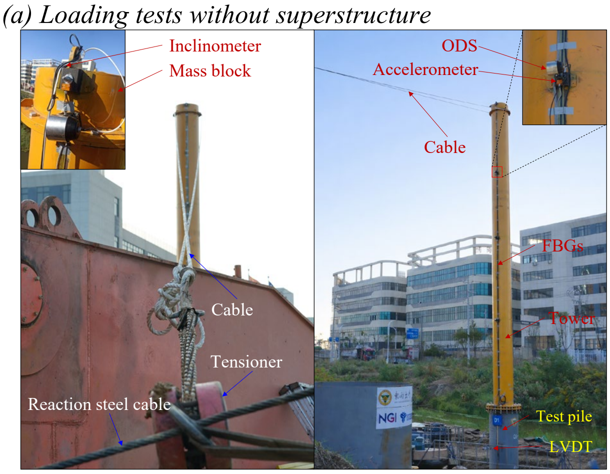

(b) Free-vibration tests with superstructure

(c) Forced loading tests with superstructure

Figure 3. Testing set-ups for the three types of field tests

The actuator is connected to the testing pile and the reaction through clamps at both ends and extension rods, as illustrated in Figure 3. A load cell was installed at the connection between the actuator and the extension rod. Four linear variable differential transformers (LVDTs) were installed on both sides of the testing pile between the loading point and the ground surface. Inclinometers were mounted either on the clamp attached to the test pile or on the top of the lumped mass. Five optical displacement sensors (ODS) were installed along the height of the tower, with accelerometers mounted at the same positions. Fibre Bragg Grating (FBG) strain sensors were mounted along the length of the testing pile and the tower. In addition, cameras were installed to monitor the soil-pile interface during the tests.

2.3 Monotonic tests without superstructure

The monotonic loading tests without the superstructure were conducted to investigate the stiffness of the soil-pile interaction and to determine the ultimate lateral capacity (F_u) of the monopile, which was subsequently used as a reference for defining the load levels in the cyclic loading tests. The monotonic tests were performed under displacement control at a loading rate of 3 mm/min. The load was applied at a height of 1 m above the unexcavated mudline (or 2 m above the excavated mudline). Details of the instrumentation layout are shown in Figure 3(a).

Two monotonic tests were carried out in total, one on a 9 m long pile and the other on a 13 m long pile. The loading procedure typically comprised two unloading-reloading loops during the test to observe changes in the soil-pile system stiffness, as illustrated by Figure 4.

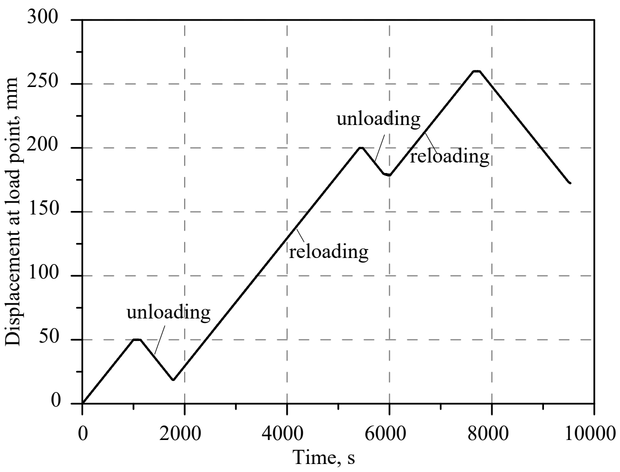

Figure 4. Monotonic test regime

2.4 Cyclic loading tests without superstructure

The cyclic loading tests without the superstructure were conducted to investigate the cyclic stiffness and damping of the soil-pile interaction under different cyclic load levels. The tests were performed under force control using a sinusoidal loading signal with a frequency of 0.1 Hz.

During the tests, five consecutive cyclic loading episodes were applied. The first episode comprised 100 loading cycles, while each of the subsequent episodes consisted of 200 cycles. The cyclic load amplitudes were set to $0.05F_u$, $0.1F_u$, $0.2F_u$, $0.3F_u$ and $0.4\ F_u$, respectively, as shown in Figure 5. Within each episode, the load amplitude was kept constant, whereas it was increased progressively between successive episodes. The tests were terminated after all predefined cyclic loading episodes had been completed. The loading apparatus and monitoring system were identical to those used in the monotonic test regime, except for the test pile.

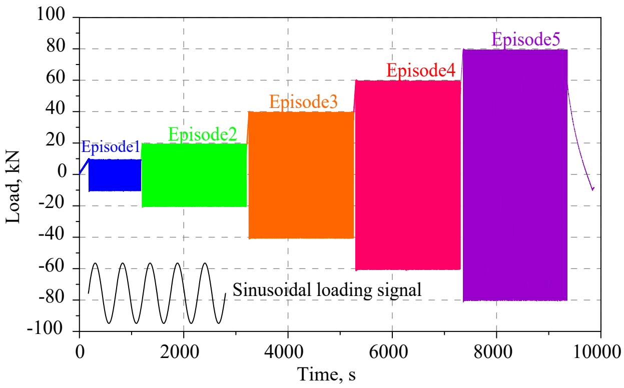

Figure 5. Cyclic test regime

2.5 Free vibration tests with superstructure

The free vibration tests with the superstructure were conducted to investigate the initial stiffness and damping of the soil-pile interaction by measuring the natural frequencies and damping ratios of the pile-soil-tower-lumped mass system. The testing procedure and instrumentation layout are shown in Figure 3(b).

During the tests, a prescribed lateral displacement was first imposed at the top of the tower (i.e., at the location of the lumped mass) using a cable-tensioner system. The imposed displacement was measured using the ODS at the top of tower. The cable was then suddenly released. As the cable was suspended from the top of the tower rather than being fixed, it bounced off from the wind turbine system immediately upon release, as illustrated in Figure 6, thereby avoiding any influence of the cable on the dynamic response of the system. The dynamic responses at different locations of the system were measured using a combination of ODSs, accelerometers and LVDTs.

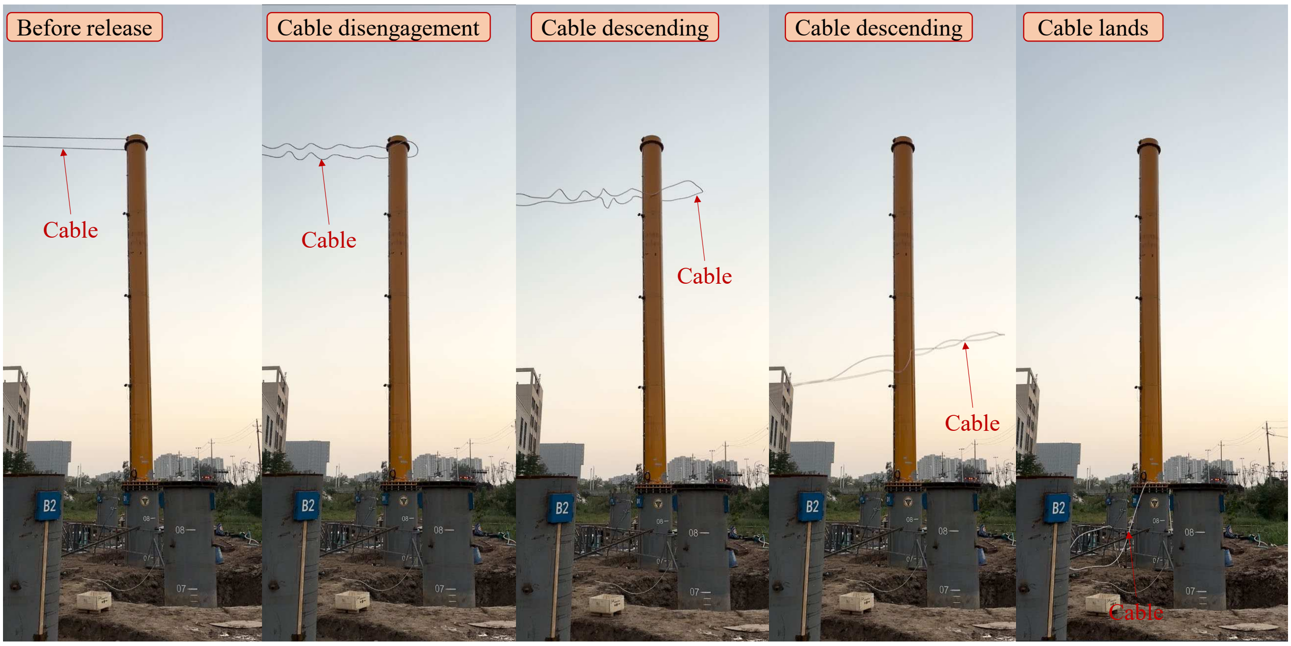

Figure 6. Free vibration test regime

2.6 Forced excitation tests with the superstructure

The forced excitation tests with the superstructure were conducted to investigate the dynamic stiffness and damping of the soil-pile interaction, as well as the load-reduction effects of soil-pile damping on the dynamic response of the wind turbine system. The tests were performed under force control using a symmetric sinusoidal loading signal. The loading programme for a representative test is summarised in Table 2.

Table 2. The loading programme for a representative forced excitation test.

No.	Amplitude kN	Frequency Hz	No. of cycles -
1	0.05F_u, 10kN	0.1, 0.5, 1, 1.5, 2.5, 3, 4	50
2	0.075F_u, 15kN	0.1, 0.5, 1, 1.5, 2.5, 3, 4	50
3	0.1F_u, 20kN	0.1, 0.5, 1, 1.5, 2.5, 3, 4	50
4	0.2F_u, 40kN	0.1, 0.5, 1, 1.5, 2.5, 3, 4	50
5	0.3F_u, 60kN	3, 1	50
7	0.4F_u, 80kN	3, 1	50

The frequency sweep tests were carried out under four different cyclic load levels over a frequency range of 0.1-4 Hz. For each frequency, the system was excited by 50 cycles. The free vibration tests identified a first-order eigenfrequency of approximately 1.9 Hz. The forced excitation tests therefore examined the system dynamics under loading frequencies both lower and higher than its eigenfrequency. Within each loading episode, the cyclic load amplitude and frequency were kept constant. Upon completion of each episode, the subsequent loading was applied only after vibration of the entire system had come to a complete stop. Details of the instrumentation layout are shown in Figure 3(c).

3 RESULTS

3.1 Results of representative monotonic loading test without superstructure

In this section, results of monotonic loading test on the short pile (6 m penetration measured from the excavated mudline) are presented. Figure 7 presents the LVDT measurements obtained from four LVDTs installed at two different elevations. The results show excellent consistency between the LVDTs located on opposite sides of the pile at the same elevation. Based on these measurements, the pile displacement at the loading point was derived. Together with the force measurements from the load cell, the force-displacement relationship at the loading point was obtained, as shown in Figure 8.

Class A prediction using 3D FEA is also included in Figure 8. Excellent agreement is observed between the experimental results and the 3D FEA (Fu et al.,2020) prediction, both in terms of the force-displacement response at the loading point and the bending moment response along the pile (Figure 9). This agreement further demonstrates the reliability of the experimental data and provides a robust data basis for the further validation of the *p-y* method proposed by Zhang and Andersen (2017).

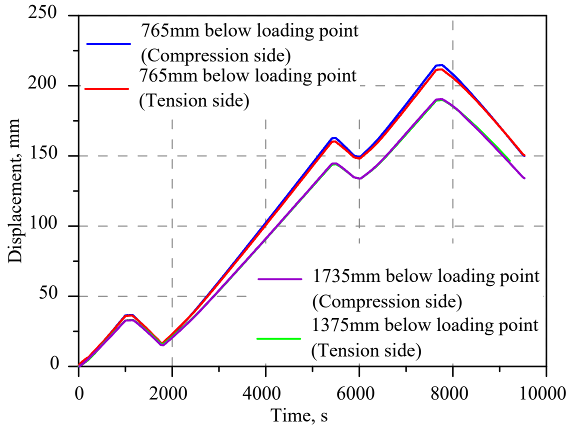

Figure 7. LVDT results at different locations.

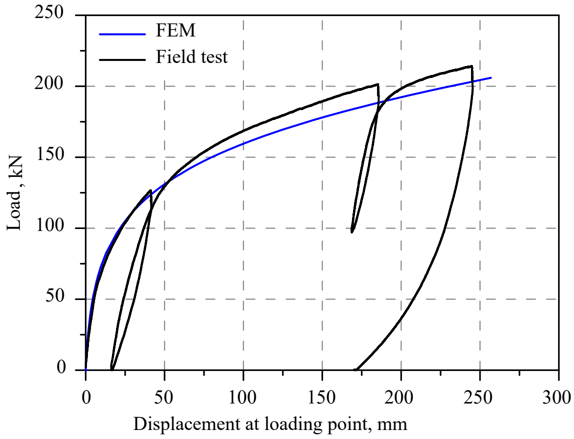

Figure 8. Load vs displacement at loading point.

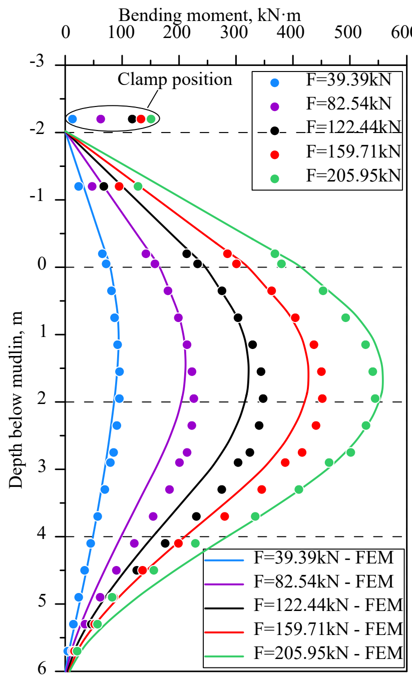

Figure 9. Bending moment results along the pile.

3.2 Results of cyclic loading test without superstructure

Figure 10 compares the force-displacement responses at the loading point obtained from the monotonic loading test and the cyclic loading test at different cyclic amplitudes. Overall, the cyclic soil-pile interaction stiffness during the first cycle of each loading episode is slightly higher than the corresponding static stiffness, indicating a moderate rate effect. Nevertheless, good overall consistency between the monotonic and cyclic responses is observed. With increasing cyclic load amplitude, cyclic degradation of the soil-pile system becomes evident when the load amplitude reaches $0.3F_u$ and $0.4F_u$, with the effect being particularly pronounced at $0.4F_u$.

Further insight is provided in Figure 11, which presents the evolution of damping ratio with the number of cycles for different cyclic amplitudes. For the first three loading episodes, the damping ratio remains nearly constant with cycle number. In contrast, for episodes with cyclic amplitudes of $0.3F_u$ and $0.4F_u$, the damping ratio increases progressively with the number of cycles. This behaviour reflects the cyclic degradation of the soil-pile system during these two episodes, leading to widening of the hysteresis loops.

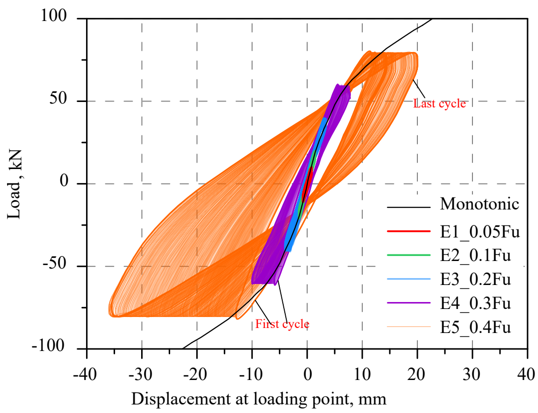

Figure 10. Load vs displacement responses at the loading point.

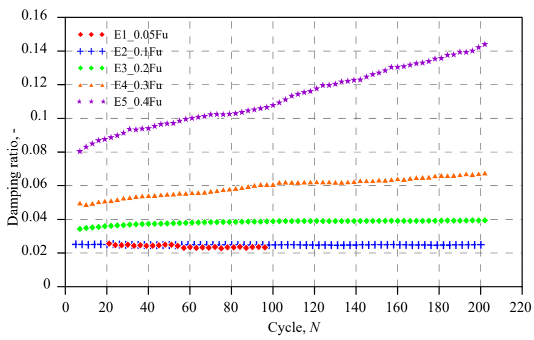

Figure 11. Evolution of damping ratio with number of cycles

3.3 Results of free vibration test with superstructure

Figure 12 presents the displacement responses measured at different elevations along the tower during a representative free vibration test. Owing to space limitations, only the first 15 oscillation cycles are shown. Overall, good consistency is observed among the displacement measurements obtained from the optical displacement sensors at different elevations.

The natural frequency derived from the free-vibration test is 1.904 Hz. This is in good agreement with Class A prediction which estimated 1.948 Hz.

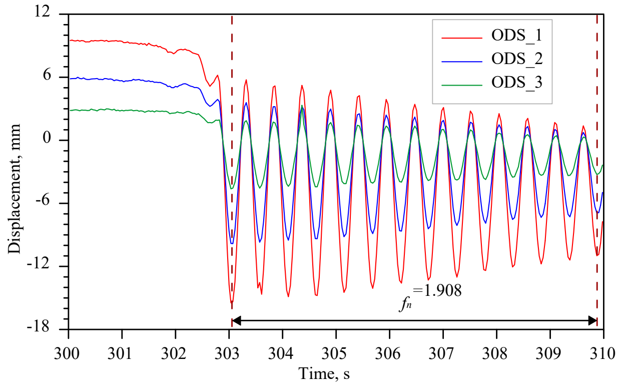

Figure 12. The results of optical displacement sensors in a free vibration tests

3.4 Results of forced excitation test with superstructure

Figure 13 presents the force-displacement responses at the loading point obtained from frequency sweep tests conducted at a fixed loading amplitude. The maximum displacement response is observed for 1.5 Hz, which is close to the natural frequency of 1.904 Hz, exhibiting the most pronounced dynamic amplification. Whereas the least displacement response is observed for 2.5 Hz, exhibiting dynamic reduction.

Another notable feature is that the force-displacement hysteresis loops become progressively wider with increasing loading frequency, implying an increase in the damping ratio of the wind turbine system. This behaviour suggests that, in addition to hysteretic damping, the radiation damping may become increasingly more significant. A quantitative assessment of this contribution and examination of its relevance to practical engineering is beyond the scope of the present paper and will be explored in future publications.

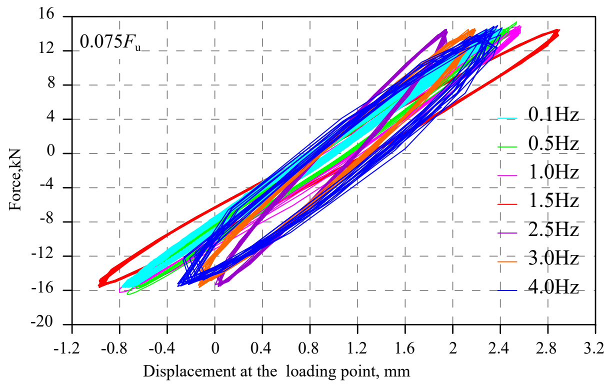

(a) F_{cy}=0.075F_u

Figure 13. Representative results from force excitation test with superstructure

4 CONCLUSIONS

A field-based, medium-scale (1:10) physical model testing programme was carried out at a homogeneous marine clay site to characterise soil-pile interaction stiffness and damping relevant to monopile-supported offshore wind turbine structures. The programme includes both monotonic and cyclic loading tests without the superstructure as well as free-vibration and forced excitation tests with the superstructure. Preliminary interpretation of the test results suggests excellent agreement with theoretical predictions. Further interpretations of the test results and validation of theoretical models are currently ongoing and will be published in future publications.

ACKNOWLEDGEMENTS

The authors wish to gratefully acknowledge the vision, leadership and financial support by Goldwind who made it possible to carry out this research.

REFERENCES

Barzan, M. and Igoe, D. (2024). Determination of foundation damping coefficients for monopile supported offshore wind turbines. *The 28th European Young Geotechnical Engineers Conference*.

Burd, H. J., Abadie, C. N., Byrne, B. W., Houlsby, G. T., Martin, C. M., McAdam, R. A., ... and Andrade, M. P. (2020a). Application of the PISA design model to mo nopiles embedded in layered soils. *Géotechnique*, 70(1 1), 1067-1082. https://doi.org/10.1680/jgeot.20.PISA.009

Burd, H. J., Taborda, D. M., Zdravković, L., Abadie, C. N., Byrne, B. W., Houlsby, G. T., ... and Potts, D. M. (2020b). PISA design model for monopiles for offshore wind turbines: application to a marine sand.

Géotechnique, 70(11), 1048-1066. https://doi.org/10.1680/jgeot.18.P.277

Byrne, B. W., Houlsby, G. T., Burd, H. J., Gavin, K. G., Igoe, D. J., Jardine, R. J., ... and Zdravković, L. (2020). PISA design model for monopiles for offshore wind turbines: application to a stiff glacial clay till. *Géotechnique*, 70(11), 1030-1047. https://doi.org/10.1680/jgeot.18.P.255

Carswell, W., Johansson, J., Løvholt, F., Arwade, S. R., Madshus, C., Degroot, D. J. and Myers, A. T. (2015). Foundation damping and the dynamics of offshore wind turbine monopiles. *Marine Structures*, 80, 724–736. https://doi.org/10.1016/j.renene.2015.02.058

Carswell, W., Arwade, S. R., Johansson, J. and DeGroot, D. J. (2022). Influence of foundation damping on offshore wind turbine monopile design loads. *Marine Structures*, 83, 103154. https://doi.org/10.1016/j.marstruc.2021.103154

Fontana, C. M., Carswell, W., Arwade, S. R., DeGroot, D. J., and Myers, A. T. (2015). Sensitivity of the dynamic response of monopile-supported offshore wind turbines to structural and foundation damping. *Wind Engineering*, 39(6). https://doi.org/10.1260/0309-524X.39.6.609

Fu, D., Zhang, Y., Aamodt, K. K. and Yan, Y. (2020). A multi-spring model for monopile analysis in soft clays. *Marine Structures*, 72, 102768. https://doi.org/10.1016/j.marstruc.2020.102768

Guo, P., Ling, H., Zhang, Y., and Di, T. (2024). Modelling of foundation damping in time-domain analysis of monopile supported offshore wind turbine structures. *Marine Structures*, 98, 103672.

Guo, P., Zhang, Y. and Di, T. (2025a). Hysteretic foundation damping model for large-diameter monopile supporting offshore wind turbines. *Marine Georesources & Geotechnology*, 1-13. https://doi.org/10.1080/1064119X.2025.2539490

Guo, P., Zhang, Y., and Bi, Q. (2025b). Characteristics of the Damping Ratio of Undisturbed Offshore Silty Clay in Eastern Guangdong, China. *Applied Sciences*, 15(9), 4954. https://doi.org/10.3390/app15094954

GWEC, *5 Global Offshore Wind Report 2025*. Global Wind Energy Council, Brussels, Belgium.

Jindal, S., Rahmanli, U., Aleem, M., Cui, L., Jalbi, S., and Bhattacharya, S. (2024a). Identification of soil damping for stiff piles based on experiments: Methodology and results. *Ocean engineering*, 301, 117124.

Jindal, S., Rahmanli, U., Aleem, M., Cui, L., & Bhattacharya, S. (2024b). Identification of soil damping for stiff piles based on experiments: Soil damping curves from physical model tests. *Ocean Engineering*, 310, 118497.

Lai, Y., Wang, L., Zhang, Y. and Hong, Y. (2021). Site-specific soil reaction model for monopiles in soft clay based on laboratory element stress-strain curves. *Ocean Engineering*, 220, 108437. https://doi.org/10.1016/j.oceaneng.2020.108437

Linde, Ø. M. and Saeland, M. K. (2022). *Estimating modal damping due to hysteric soil behaviour and its effect on fatigue response of offshore wind structures on jackets and monopiles*. MSc. thesis, Norwegian University of Science and Technology, Trondheim, Norway.

Page, A. M., Norén-Cosgriff, K., Skau, K. S., & Kaynia, A. M. (2019, June). REDWIN foundation models for integrated dynamic analyses of offshore wind turbines. In *International Conference on Offshore Mechanics and Arctic Engineering* (Vol. 58899, p. V010T09A073). American Society of Mechanical Engineers.

Page, A. M., Næss, V., De Vaal, J. B., Eiksund, G. R., & Nygaard, T. A. (2019). Impact of foundation modelling in offshore wind turbines: Comparison between simulations and field data. *Marine Structures*, 64, 379-400. https://doi.org/10.1016/j.marstruc.2018.11.010

Rezaei, R., Fromme, P. and Duffour, P. (2018). Fatigue life sensitivity of monopile-supported offshore wind turbines to damping. *Renewable Energy*, 123, 450-459.

Shirzoi, A. G., Ma, Z., Zhang, B. N., Dai, S. and Bo, H. (2024). Investigation of soil damping for offshore wind turbine monopile-soil system in stiff clay on elastoplastic-damage model. *Marine Georesources and Geotechnology*, 1-16. https://doi.org/10.1080/1064119X.2024.2372816

Suryasentana, S. K. and Lehane, B. M. (2016). Updated CPT-based p–y formulation for laterally loaded piles in cohesionless soil under static loading. *Géotechnique*, 66(6), 445-453. https://doi.org/10.1680/jgeot.14.P.156

Wang, H., Lehane, B. M., Bransby, M. F., Askarinejad, A., Wang, L. Z. and Hong, Y. (2022). A simple rotational spring model for laterally loaded rigid piles in sand. *Marine Structures*, 84, 103225. https://doi.org/10.1016/j.marstruc.2022.103225

Zhang, Y. and Andersen, K. H. (2017). Scaling of lateral pile p-y response in clay from laboratory stress-strain curves. *Marine Structures*, 53, 124–135. https://doi.org/10.1016/j.marstruc.2017.02.002

Zhang, Y. and Andersen, K. H. (2019). Soil reaction curves for monopiles in clay. *Marine Structures*, 65, 94–113. https://doi.org/10.1016/j.marstruc.2018.12.009

Zhang, Y., Aamodt, K. K. and Kaynia, A. M. (2021). Hysteretic damping model for laterally loaded piles. *Marine Structures*, 76, 102896. https://doi.org/10.1016/j.marstruc.2020.102896

Zhang, Y., Chen, J., Hu, S., Zhang, H., and Kaynia, A. M. (2023). Hysteretic damping of soils for well conductor fatigue analysis. *Marine Structures*, 89, 103392. https://doi.org/10.1016/j.marstruc.2023.103392